Study of the effect of myofibrillar misalignment on the sarcomeric SHG intensity pattern

Denis Rouède,[1,*] Jean-Jacques Bellanger,[2,3] Gaëlle Recher,[4] and François Tiaho[5]

[1]*Institut de Physique de Rennes, Département d'Optique, UMR UR1-CNRS 6251, Université de Rennes1, Campus de Beaulieu, 35042 Rennes CEDEX, France*
[2]*LTSI, Université de Rennes1, Rennes, F-35000, France*
[3]*INSERM, U1099, Rennes, F-35000, France*
[4]*Neurobiologie et développement, CNRS UPR 3294, 91198 Gif-Sur-Yvette CEDEX, France*
[5]*IRSET, UMR UR1-INSERM U1085, Université de Rennes1, Campus de Beaulieu, 35042 Rennes CEDEX, France*
[*]*denis.rouede@univ-rennes1.fr*

Abstract: We present a theoretical simulation of the sarcomeric SHG intensity pattern (SHG-IP) that takes into account myofibrillar misalignment that is experimentally observed in SHG images of proteolysed muscles. The model predicts that myofibrillar displacement results in the conversion from one peak (1P) to two peaks (2P) sarcomeric SHG-IP in agreement with experimental results. This study suggests that sarcomeric SHG-IP is a powerful tool for mapping spatial myofibrillar displacement and its related excitation-contraction disruption that could occur during muscle physiological adaptation and disease.

©2013 Optical Society of America

OCIS codes: (180.4315) Nonlinear microscopy; (190.4160) Multiharmonic generation; (170.3880) Medical and biological imaging.

References and links

1. P. J. Campagnola and L. M. Loew, "Second-harmonic imaging microscopy for visualizing biomolecular arrays in cells, tissues and organisms," Nat. Biotechnol. **21**(11), 1356–1360 (2003).
2. W. R. Zipfel, R. M. Williams, and W. W. Webb, "Nonlinear magic: multiphoton microscopy in the biosciences," Nat. Biotechnol. **21**(11), 1369–1377 (2003).
3. O. Friedrich, M. Both, C. Weber, S. Schürmann, M. D. H. Teichmann, F. von Wegner, R. H. A. Fink, M. Vogel, J. S. Chamberlain, and C. Garbe, "Microarchitecture Is Severely Compromised but Motor Protein Function is Preserved in Dystrophic mdx Skeletal Muscle," Biophys. J. **98**(4), 606–616 (2010).
4. M. E. Llewellyn, R. P. Barretto, S. L. Delp, and M. J. Schnitzer, "Minimally invasive high-speed imaging of sarcomere contractile dynamics in mice and humans," Nature **454**(7205), 784–788 (2008).
5. V. Nucciotti, C. Stringari, L. Sacconi, F. Vanzi, L. Fusi, M. Linari, G. Piazzesi, V. Lombardi, and F. S. Pavone, "Probing myosin structural conformation in vivo by second-harmonic generation microscopy," Proc. Natl. Acad. Sci. U.S.A. **107**(17), 7763–7768 (2010).
6. S. V. Plotnikov, A. M. Kenny, S. J. Walsh, B. Zubrowski, C. Joseph, V. L. Scranton, G. A. Kuchel, D. Dauser, M. Xu, C. C. Pilbeam, D. J. Adams, R. P. Dougherty, P. J. Campagnola, and W. A. Mohler, "Measurement of muscle disease by quantitative second-harmonic generation imaging," J. Biomed. Opt. **13**(4), 044018 (2008).
7. E. Ralston, B. Swaim, M. Czapiga, W. L. Hwu, Y. H. Chien, M. G. Pittis, B. Bembi, O. Schwartz, P. Plotz, and N. Raben, "Detection and imaging of non-contractile inclusions and sarcomeric anomalies in skeletal muscle by second harmonic generation combined with two-photon excited fluorescence," J. Struct. Biol. **162**(3), 500–508 (2008).
8. F. Tiaho, G. Recher, and D. Rouède, "Estimation of helical angles of myosin and collagen by second harmonic generation imaging microscopy," Opt. Express **15**(19), 12286–12295 (2007).
9. G. Recher, D. Rouède, P. Richard, A. Simon, J.-J. Bellanger, and F. Tiaho, "Three distinct sarcomeric patterns of skeletal muscle revealed by SHG and TPEF Microscopy," Opt. Express **17**(22), 19763–19777 (2009).
10. G. Recher, D. Rouède, E. Schaub, and F. Tiaho, "Skeletal muscle sarcomeric SHG patterns photo-conversion by femtosecond infrared laser," Biomed. Opt. Express **2**(2), 374–384 (2011).
11. G. Recher, D. Rouède, C. Tascon, L. A. D'Amico, and F. Tiaho, "Double-band sarcomeric SHG pattern induced by adult skeletal muscles alteration during myofibrils preparation," J. Microsc. **241**(2), 207–211 (2011).
12. D. Rouède, G. Recher, J. J. Bellanger, M. T. Lavault, E. Schaub, and F. Tiaho, "Modeling of Supramolecular Centrosymmetry Effect on Sarcomeric SHG Intensity Pattern of Skeletal Muscles," Biophys. J. **101**(2), 494–503 (2011).

#186253 - $15.00 USD Received 5 Mar 2013; revised 19 Apr 2013; accepted 20 Apr 2013; published 2 May 2013
(C) 2013 OSA

13. D. Rouède, J. J. Bellanger, E. Schaub, G. Recher, and F. Tiaho, "Theoretical and experimental SHG angular intensity patterns from healthy and proteolysed muscles," Biophys. J. **104**(9), 1959–1968 (2013).
14. L. S. Song, E. A. Sobie, S. McCulle, W. J. Lederer, C. W. Balke, and H. Cheng, "Orphaned ryanodine receptors in the failing heart," Proc. Natl. Acad. Sci. U.S.A. **103**(11), 4305–4310 (2006).
15. A. R. Lyon, K. T. MacLeod, Y. Zhang, E. Garcia, G. K. Kanda, M. J. Lab, Y. E. Korchev, S. E. Harding, and J. Gorelik, "Loss of T-tubules and other changes to surface topography in ventricular myocytes from failing human and rat heart," Proc. Natl. Acad. Sci. U.S.A. **106**(16), 6854–6859 (2009).
16. V. Dubowitz and C. A. Sewry, *Muscle Biopsy: A Practical Approach*, 3rd Ed. (London, 2007).
17. R. M. Lovering, A. O'Neill, J. M. Muriel, B. L. Prosser, J. Strong, and R. J. Bloch, "Physiology, structure, and susceptibility to injury of skeletal muscle in mice lacking keratin 19-based and desmin-based intermediate filaments," Am. J. Physiol. Cell Physiol. **300**(4), C803–C813 (2011).
18. Z. Li, M. Mericskay, O. Agbulut, G. Butler-Browne, L. Carlsson, L. E. Thornell, C. Babinet, and D. Paulin, "Desmin is essential for the tensile strength and integrity of myofibrils but not for myogenic commitment, differentiation, and fusion of skeletal muscle," J. Cell Biol. **139**(1), 129–144 (1997).
19. M. Both, M. Vogel, O. Friedrich, F. von Wegner, T. Künsting, R. H. A. Fink, and D. Uttenweiler, "Second harmonic imaging of intrinsic signals in muscle fibers in situ," J. Biomed. Opt. **9**(5), 882–892 (2004).
20. D. Rhee, J. M. Sanger, and J. W. Sanger, "The premyofibril - evidence for its role in myofibrillogenesis," Cell Motil. Cytoskeleton **28**(1), 1–24 (1994).
21. J. W. Sanger, J. S. Wang, B. Holloway, A. P. Du, and J. M. Sanger, "Myofibrillogenesis in Skeletal Muscle Cells in Zebrafish," Cell Motil. Cytoskeleton **66**(8), 556–566 (2009).
22. J. Mertz and L. Moreaux, "Second-harmonic generation by focused excitation of inhomogeneously distributed scatterers," Opt. Commun. **196**(1-6), 325–330 (2001).
23. N. Prent, C. Green, C. Greenhalgh, R. Cisek, A. Major, B. Stewart, and V. Barzda, "Intermyofilament dynamics of myocytes revealed by second harmonic generation microscopy," J. Biomed. Opt. **13**(4), 041318 (2008).
24. I. Freund, "Nonlinear diffraction," Phys. Rev. Lett. **21**(19), 1404–1406 (1968).
25. I. Freund, M. Deutsch, and A. Sprecher, "Connective-tissue polarity - optical second-harmonic microscopy, crossed-beam summation, and small-angle scattering in rat-tail tendon," Biophys. J. **50**(4), 693–712 (1986).
26. P. A. Franken and J. F. Ward, "Optical harmonics and nonlinear phenomena," Rev. Mod. Phys. **35**(1), 23–39 (1963).
27. M. M. Fejer, G. A. Magel, D. H. Jundt, and R. L. Byer, "Quasi-phase-matched second harmonic generation: tuning and tolerances," IEEE J. Quantum Electron. **28**(11), 2631–2654 (1992).

1. Introduction

Second Harmonic Generation (SHG) imaging microscopy takes advantage of a nonlinear and coherent frequency-doubling optical effect inherent to very few biomolecules, i.e. collagen, myosin, tubulin that are packed in a non-centrosymmetric polycrystalline lattice [1, 2]. Hence, SHG microscopy has successfully provided direct imaging of individual sarcomeres in physiological and disease muscles [3–9]. We have previously shown that sarcomeric SHG intensity pattern (SHG-IP) was predominantly one peak (1P) in healthy tissue and two peaks (2P) in proteolysed tissue in case of mechanical and oxidative stress [10–12]. We have recently developed a theoretical model to calculate SHG intensity from a bundle of myofibrils taking account of their size and of their relative distribution [13]. In the present work, we use the result of this model to calculate SHG-IP taking into account myofibrillar misalignment experimentally observed in SHG images of proteolysed tissue. A good agreement between theoretical and experimental SHG-IPs is found. The model predicts that for resting sarcomere of length 2-2.4 µm, myofibrillar displacement greater than 0.6 µm induced 2P sarcomeric SHG-IP. This study opens new opportunity for SHG microscopy to probe disruption of the excitation contraction coupling [14, 15] at the triad junction due to structural myofibrillar disorganization as observed in several animal and human skeletal muscle gene diseases [16–18].

2. Materials and methods

2.1 Sample preparation

Muscle tissues were obtained from gastrocnemius of adult *Xenopus laevis* (National breeding facility of xenopus animals in Rennes, France). Mature male animals were anesthetized by immersion for 10-15 min in 2% phenoxyethanol (Sigma-Aldrich). Dissected muscles were incubated in Mark's modified Ringer (MMR) for 3 or 24 hours before fixation in MMR

#186253 - $15.00 USD Received 5 Mar 2013; revised 19 Apr 2013; accepted 20 Apr 2013; published 2 May 2013
(C) 2013 OSA

containing 4% paraformaldehyde (PFA). Dissected muscles were either free or elongated and tied to rigid plastic rods before and during fixation. We found that 3 hours elongation in MMR results in mild proteolysis whereas 24 hours incubation in MMR results in drastic proteolysis at room temperature (18-22°C). Muscles were kept overnight at 4° C in the fixative and washed several times in the appropriate buffer saline. Dissected pieces of muscle fibers (200 - 400 µm thickness) were mounted in a POC-R2 tissue culture chamber system (POC chamber system, PeCon, GmbH), in MMR and stabilized between two coverslips. Immunostaining of Z-band α-actinin were obtained as previously reported [9] from 24 hours proteolysed muscle. Briefly, 10-15 µm cryostat muscle tissue sections, α-actinin primary antibody (1:100, mouse monoclonal IgM, ab9465, Abcam, Cambridge, MA, USA) and Alexa Fluor 488 secondary antibody (1:100, goat antimouse IgG, A11029, Molecular Probes, Eugene, OR, USA) were used.

2.2 SHG imaging system

SHG imaging system has been described elsewhere [12, 13]. It consists in a confocal Leica TCS SP2 scanning head (Leica Microsystems, Mannheim, Germany) mounted on a Leica DMIRE2 inverted microscope and equipped with a MAITAI Spectra Physics femtosecond laser (Spectra Physics, Santa Clara, CA, USA). Water immersion objective (Olympus LUMFL 60W × 1.1 NA) (Olympus, Tokyo, Japan) and multi-immersion S1 (NA = 0.90-1.4) Leica condenser were used respectively for applying 10-20 mW of 940 nm excitation at the sample and for collection. BG39 bandpass and 470 nm IR (10 nm FWHM) filters were placed before the PMT. All specimens were positioned on the *x*, *y* stage of the microscope with the main myofibrillar axis along *x* direction. Incident laser beam was propagating along *z* direction with input polarization along y direction. Beam waist w_{xy} and w_z were estimated from the two-photon excitation point spread function obtained from 0.17 µm diameter fluorescent micro beads (Molecular Probes PS-Speck Microscope Point Source Kit (P7220)). Lateral and axial FWHM were found to be $\mathrm{FWHM}_{x,y} = 0.4\ \mu m$ and $\mathrm{FWHM}_z = 2\ \mu m$ at 940 nm. $w_{xy} = 0.48\ \mu m$ and $w_z = 2.4\ \mu m$ were deduced from these values using $w_{xy,z} = \mathrm{FWHM}_{xy,z} / \sqrt{\ln 2}$ [2, 12]. Open source ImageJ (http://rsb.info.nih.gov/ij/) and UCSF Chimera (http://www.cgl.ucsf.edu/chimera/) softwares were used for respectively SHG image analysis and 3-D reconstruction.

2.3 Theoretical simulation

MATLAB (MathWorks, Natick, MA, USA) was used for simulation of the theoretical SHG-IP. Values of parameters used for the simulation are the same as in reference [13]. Transverse section of each myofibril is considered to be rectangular with size $\ell_y = \ell_z = 1\ \mu m$. Sizes of sarcomeric A- and M-bands for well ordered thick filaments within each sarcomere are respectively $A = 1.6\ \mu m$ and m = 150 nm [12]. Spatial periods of the Fourier development series are $L_x = L$, the sarcomere size and $L_y = L_z = 15\ \mu m$. Number of Fourier coefficients is set to n = 40. Refractive indices at fundamental and harmonic frequencies are taken equal $n_\omega = n_{2\omega} = 1.33$.

3. Experimental results

We have previously shown that SHG images of healthy and spontaneous post mortem proteolysed muscle tissue are respectively predominantly 1P and 2P sarcomeric SHG-IP [9]. 2P sarcomeric SHG-IP are sometimes characterized by pitchforklike SHG patterns [3, 7, 9, 19]. These patterns have been observed and interpreted as the result of mini sarcomeres associated to muscle regeneration based on immuno fluorescence images analysis [9, 20, 21]. We found that these pitchforklike SHG patterns shown in Fig. 1 significantly increase from

#186253 - $15.00 USD Received 5 Mar 2013; revised 19 Apr 2013; accepted 20 Apr 2013; published 2 May 2013
(C) 2013 OSA

10 ± 2% (n = 126 random fields) in muscles that were not elongated to 19 ± 2% (n = 119 random fields, p < 0.001) for 30% elongated muscles suggesting that they could be the result of muscle proteolysis. These typical pitchforklike SHG patterns are characterized by central double-band sarcomeric SHG pattern bordered by single-band sarcomeric SHG pattern as illustrated by a xy section of a z-stack shown in Fig. 1(a) and by the SHG-IP obtained at y = 0 µm shown in Fig. 1(d).

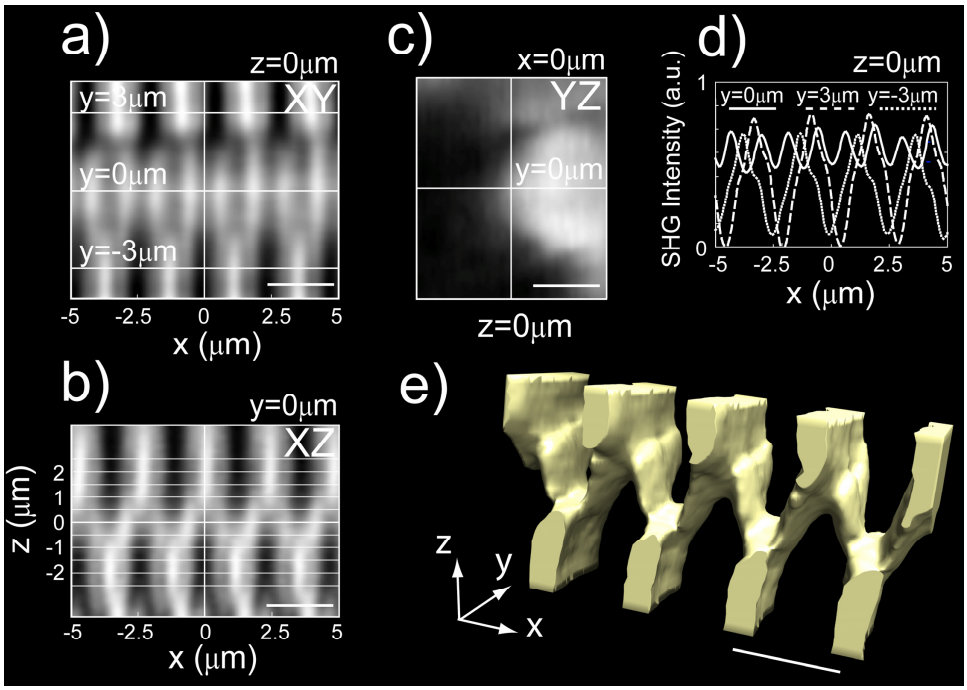


Fig. 1. SHG images and experimental SHG-IPs. (a) SHG image at the middle (z = 0µm) of a z-stack of muscle tissue that experienced 30% elongation induced 3 hours mild-proteolysis. Horizontal lines at y = 0 µm, y = 3 µm and y = - 3 µm are ROIs for SHG-IP of (d). (b) Corresponding xz view obtained at y = 0 µm. Note that horizontal full lines localized SHG images of Fig. 2(a). (c) Corresponding yz view obtained at x = 0 µm. As SHG signal originates from the A-band, note the I-band to A-band transition from left to right. (d) SHG-IPs obtained along lines y = 0 µm, y = 3 µm and y = –3 µm of (a). (e) 3-D view of the pitchforlike SHG pattern. Scale bars are 2.5 µm.

Orthogonal xz projection from the stack that is shown in Fig. 1(b) also exhibits such pattern, indicating misalignment of sarcomeric A-bands across the depth of the tissue. Such misalignment is also clearly observed in the orthogonal yz projection of Fig. 1(c). A 3-D view of the pitchforlike SHG pattern is shown in Fig. 1(e). This later is reminiscent of staircase or vernier SHG pattern first described in mouse muscle [19]. To better understand the origin of these pitchforklike SHG patterns, we compare in next section experimental SHG-IPs obtained at different z positions of the stack of Fig. 1 with theoretical ones taking account of the myofibrillar displacement observed in the stack.

4. Theoretical simulation of SHG-IP

Theoretical sarcomeric SHG-IP is obtained by calculating the total SHG intensity $I_{2\omega}^{T}$ emitted by the muscular tissue and collected by the detection optics for each position of the laser along the sarcomere. $I_{2\omega}^{T} = \int I_{2\omega}(\boldsymbol{r}) d\Omega$ is obtained by angular integration over the condenser aperture of the far-field SHG intensity $I_{2\omega}(\boldsymbol{r})$ emitted in direction $\boldsymbol{r}$. If we consider

#186253 - $15.00 USD Received 5 Mar 2013; revised 19 Apr 2013; accepted 20 Apr 2013; published 2 May 2013
(C) 2013 OSA

that myofibrils are parallel to x direction and that incident laser beam is propagating along z direction with input polarization along y direction, $I_{2\omega}(\boldsymbol{r})$ is given in spherical coordinates r, θ, φ by [12, 13]

$$\boldsymbol{I}_{2\omega}(\boldsymbol{r}) = \tfrac{\omega^4}{r^2 c^4}\chi_{15}^2 I_\omega^2 \times \left(1-\sin^2\theta\cos^2\varphi\right)\times\left|\sum_f g^f(\theta,\varphi)\right|^2 \qquad (1)$$

where summation is made over all myofibrils f within the focusing volume. I_ω is the intensity of the incident IR beam and χ_{15} is the uniform second-order nonlinear optical susceptibility coefficient involved in the interaction. $g^f(\theta,\varphi)$ is the Fourier transform of the spatial modulation function $M^f(x,y,z)$ of the second-order nonlinear optical susceptibility $\chi_{15}^f(x,y,z) = M^f(x,y,z)\,\chi_{15}$ for each myofibril f weighted by the square of the Gaussian amplitude of the excitation field [13]

$$g^f(\theta,\varphi) = \int e^{-i\left(k_x^{2\omega}x + k_y^{2\omega}y + k_z^{2\omega}z\right)} \times M^f(x,y,z) \times e^{-2\frac{x^2+y^2}{w_{xy}^2} - 2\frac{z^2}{w_z^2} + 2i\xi k_z^\omega z}\, dx\, dy\, dz \quad . \qquad (2)$$

$\boldsymbol{k}^\omega = k^\omega(0,0,1)$ and $\boldsymbol{k}^{2\omega} = k^{2\omega}\left(\sin\theta\cos\varphi, \sin\theta\sin\varphi, \cos\theta\right)$ are wave vectors of respectively the fundamental and harmonic waves in the laboratory coordinates x,y,z. $\xi = 1-(k^\omega z_r)^{-1}$ is a coefficient whose value is driven by the Rayleigh range $z_r = \pi n_\omega w_{xy}^2 \lambda_\omega^{-1}$ which represents the reduction $(\xi < 1)$ of the effective axial propagation wave vector $\boldsymbol{k}^\omega$ of the incident wave caused by the phase anomaly or Gouy shift due to focusing [12, 22]. Beam waist w_{xy} and w_z are obtained from the two-photon excitation PSF (see Materials and methods). To simplify Fourier transform calculation, we consider that each myofibril is rectangular with size ℓ_y, ℓ_z respectively in y and z directions such that $M^f(x,y,z) = M_x^f(x)M_y^f(y)M_z^f(z)$ is factorizable. Using three developments in Fourier series $M_\eta^f(\eta) = \sum_{n\in\mathbb{Z}} c^f{}_{\eta n}\, e^{iG_{\eta n}\eta}$ $(\eta = x,y,z)$, Eq. (2) results in

$$g^f(\theta,\varphi) = u \times \sum_{n\in\mathbb{Z}} c_{xn}^f e^{-\frac{1}{8}w_{xy}^2\left(k_x^{2\omega}-G_{xn}\right)^2} \times \sum_{n\in\mathbb{Z}} c_{yn}^f e^{-\frac{1}{8}w_{xy}^2\left(k_y^{2\omega}-G_{yn}\right)^2} \times \sum_{n\in\mathbb{Z}} c_{zn}^f e^{-\frac{1}{8}w_z^2\left(k_z^{2\omega}-2\xi k_z^\omega-G_{zn}\right)^2} \qquad (3)$$

with $u = \left(\frac{\pi}{2}\right)^{3/2} w_{xy}^2 w_z$ and where $G_{\eta n} = 2\pi n L_\eta^{-1}$ is the $\eta = x,y,z$ component of the wave vector of order n of the Fourier development series with spatial period $L_y = L_z$ and $L_x = L$, the sarcomere size. Fourier coefficient $c^f{}_{\eta n} = L_\eta^{-1}\int_{-L_\eta/2}^{L_\eta/2} M^f(\eta)\, e^{-iG_{\eta n}\eta} d\eta$ $(\eta = x,y,z)$ of order n is given for each myofibril f by [12, 13]

$$\left|\begin{array}{ll} c^f{}_{xn} & = \frac{-2i}{\pi n}\sin\left(\frac{1}{4}G_{xn}(A-m)\right)\times\sin\left(\frac{1}{4}G_{xn}(A+m)\right)\times\exp(-iG_{xn}\Delta_x^f), \quad n\in\mathbb{Z},\ n\neq 0 \\ & = 0, \quad n = 0 \\ c^f{}_{\eta n} & = \frac{1}{\pi n}\sin\left(\frac{1}{2}G_{\eta n}\ell_\eta\right)\times\exp(-iG_{\eta n}\Delta^f{}_\eta), \quad n\in\mathbb{Z},\ n\neq 0,\ \eta = y,z \\ & = \ell_\eta L_\eta^{-1}, \quad n = 0,\ \eta = y,z \end{array}\right. \quad . \qquad (4)$$

#186253 - $15.00 USD Received 5 Mar 2013; revised 19 Apr 2013; accepted 20 Apr 2013; published 2 May 2013
(C) 2013 OSA

A and *m* are sizes of the A- and M-bands respectively (see the schematic view of the sarcomere in the inset of Fig. 3). Δ_η^f is a coefficient that is introduced to take account of a possible displacement of the center of the sarcomere of each myofibril f with respect to the center of the focus spot in $\eta = x,y,z$ direction. Finally, theoretical SHG-IP is performed by calculation of $I_{2\omega}^T$ using Eqs. (1-4) for all positions of the incident laser beam along the sarcomere width in *x* direction.

Experimental and theoretical SHG-IPs obtained from the stack of Fig. 1 are compared in the following. First, experimental SHG images obtained at different *z* positions of the stack are shown in Fig. 2(a). Experimental SHG-IPs, obtained along the horizontal line localized at the middle of each SHG image are shown in Fig. 2(b) (full lines). Second, myofibrillar schematic view of Fig. 1(b) is shown in each panel of Fig. 2(b). The first panel (z = 0) is a mimic of Fig. 1(b). This panel represents segments of 8 myofibrils (4 sarcomeres per myofibril are shown) localized in the xz plane and that are adjacent along *z* direction, parallel along *x* direction and shifted by half a sarcomere width at the center of the stack. Each following panel of Fig. 2(b) represents 8 myofibrils that are shifted by half a sarcomere width at a different ± z position from the laser focus spot that is always localized along the horizontal line at the center of each panel. Theoretical SHG-IP (dotted lines) is obtained from the myofibrillar schematic view for a laser beam focused and displaced along the horizontal line at the center of the panel considering well ordered thick filaments in each sarcomere. Good agreement between experimental (full lines) and theoretical (dotted lines, *white* color) SHG-IPs using m = 150 nm is found for all z positions. 2P sarcomeric SHG-IP is found around z = 0 where myofibrillar displacement is observed. For z = 0, minimas of the theoretical SHG-IP curve correspond to regions of low myosin density whereas maximas correspond to regions of high myosin density. Above results suggest that pitchforlike SHG patterns [19] that have been described as mini sarcomeres [9] could be the result of myofibrillar spatial displacement. Indeed, the model predicts that both well aligned mini sarcomeres and myofibrillar displacement result in the same 2P sarcomeric SHG-IP (data not shown). Based on the present simulation and TPEF α-actinin images [9], one cannot discriminate between mini sarcomeres and myofibrillar displacement. Nevertheless, in the present study, 2P sarcomeric SHG-IP is predominantly the result of myofibrillar displacement since pitchforlike structures increase by a factor of two due to proteolysis (see above).

Antiparallel reorganization of myosin molecules at the M-band has also been shown to affect the sarcomeric SHG-IP [12, 23]. We have therefore determined the additional contribution of M-band enlargement (ie increase centrosymmetry) on theoretical SHG-IP. To this aim, the M-band has been enlarged (m = 320 nm) only for the two myofibrils bordering the region of myofibrillar displacement taking into account the result of our previous report [12]. Indeed, sarcomeric SHG-IP is mostly 1P except near the region of myofibrillar displacement. Result of the simulation that is shown in Fig. 2(b) (dotted lines, *yellow* color) indicates less agreement with the experimental results suggesting no contribution of thick filaments disorder in this exemple.

We next determine the effect of myofibrillar displacement $\Delta_x^f = \pm\Delta/2$ on theoretical SHG-IP. The result is illustrated in Fig. 3 for 9 values of Δ and 6 values of sarcomere size L representing 9 × 6 panels. For each panel, upper half of myofibrils is displaced from the lower half by Δ in *x* direction and laser beam is focused along the horizontal line between the two halves at the middle of each panel. Theoretical SHG-IP is plotted (full line) in each panel with arbitrary units.

#186253 - $15.00 USD Received 5 Mar 2013; revised 19 Apr 2013; accepted 20 Apr 2013; published 2 May 2013
(C) 2013 OSA

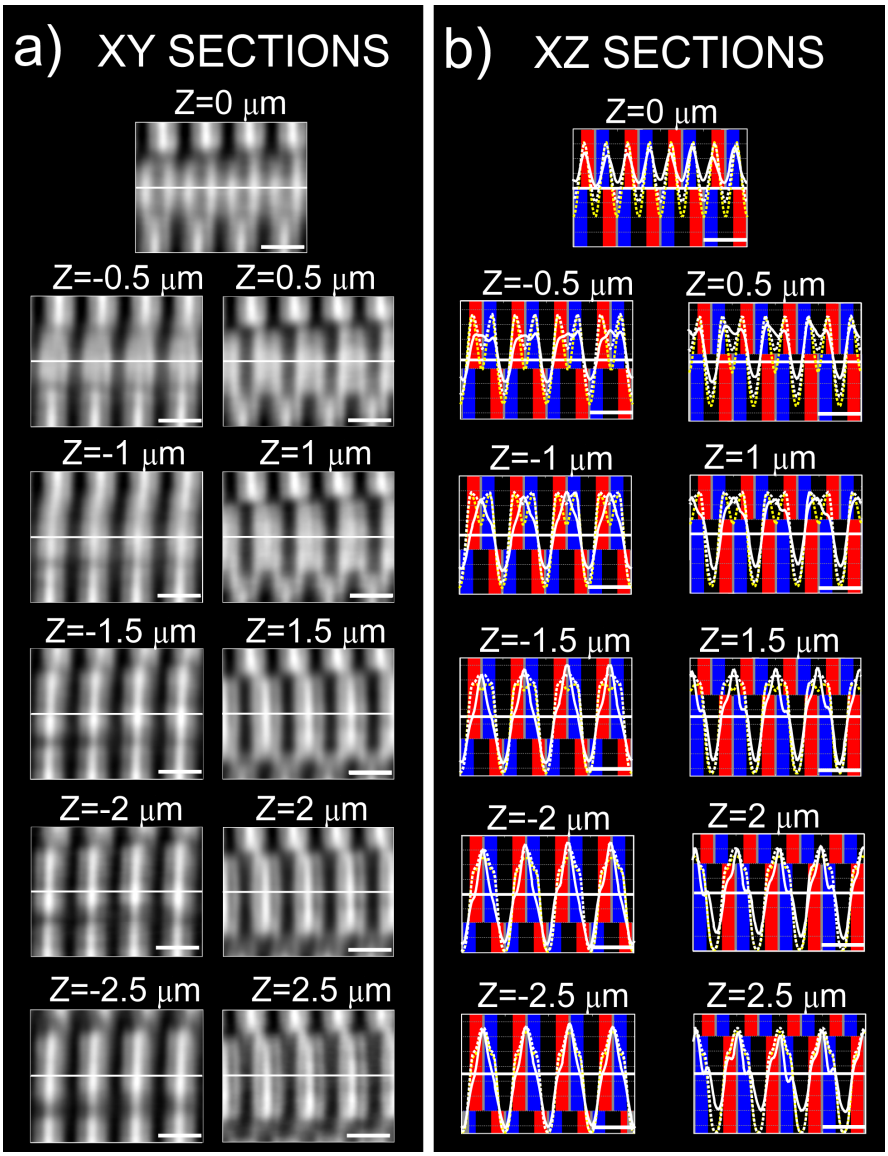


Fig. 2. SHG images and experimental/theoretical SHG-IPs. (a) SHG images are obtained at different z positions of the z-stack of Fig. 1. Note that each SHG image is labeled by its z position in the xz section of Fig. 1(b) and that z = 0 corresponds to the middle of the z-stack. (b) Experimental SHG-IPs are full lines and theoretical ones are dotted lines in *white* color (m = 150 nm for all myofibrils) and *yellow* color (m = 320 nm for the two myofibrils bordering the region of myofibrillar displacement in x direction and m = 150 nm for other myofibrils). Note that a diagram representing segments of 8 myofibrils is shown in the xz plane of each panel with a series of 4 sarcomeres consisting of A-bands (*red* and *blue* color accounting for polarity inversion) alternating with I-bands (dark color). Thin band with *grey* color at the center of each A-band corresponds to the M-band region of size m with antiparallel overlapping of myosin thick filaments where no SHG signal is produced (see also the schematic view of a sarcomere in the inset of Fig. 3). Each experimental SHG-IP is obtained along the horizontal line in the corresponding image of (a). Each theoretical SHG-IP is obtained from the corresponding myofibrillar schematic view and for a laser focus position along the horizontal line at the middle of each panel. Sarcomere size is $L = 2.5\ \mu m$ and it corresponds to the experimental mean value. SHG-IPs are drawn with arbitrary units. Scale bars are 2.5 μm.

#186253 - $15.00 USD Received 5 Mar 2013; revised 19 Apr 2013; accepted 20 Apr 2013; published 2 May 2013
(C) 2013 OSA

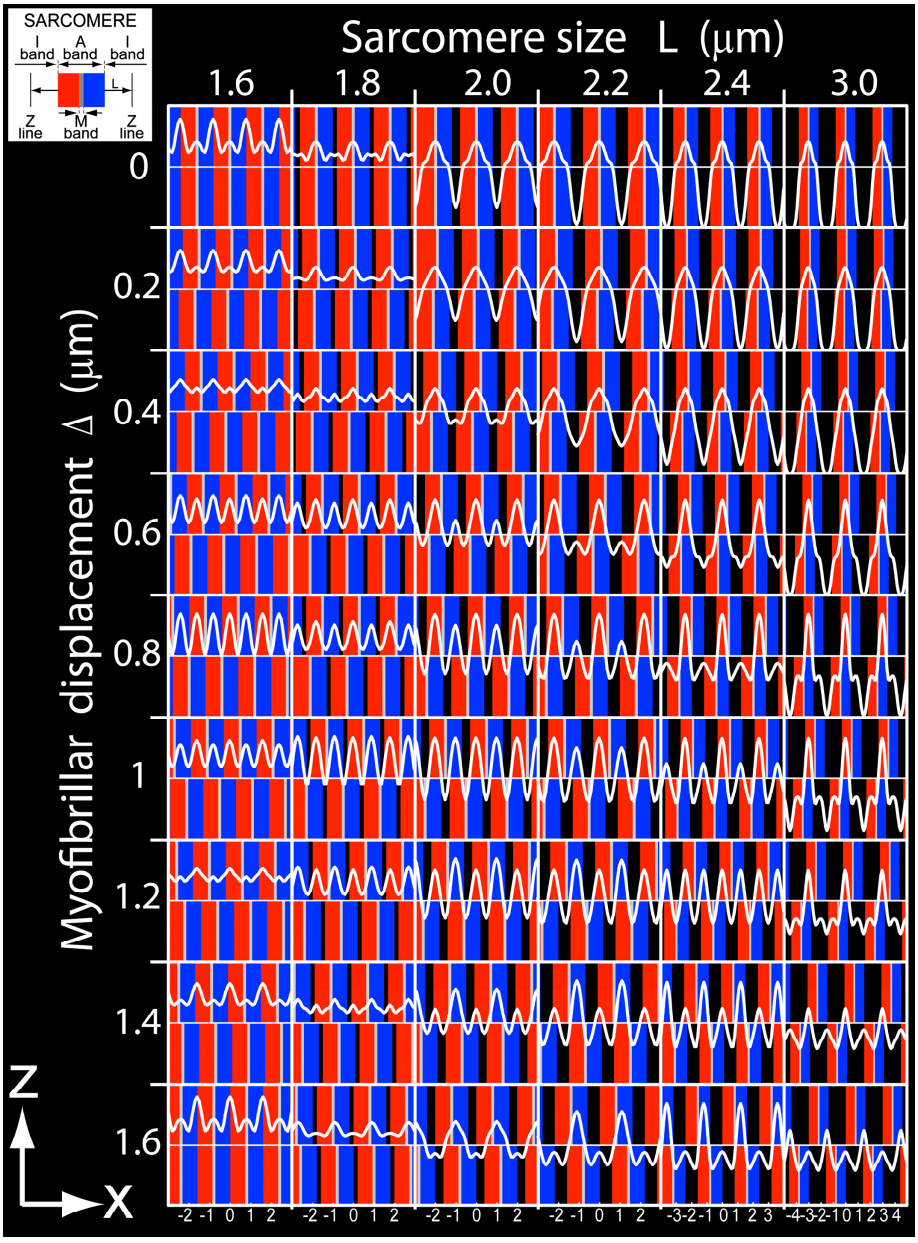


Fig. 3. Theoretical SHG-IPs as a function of sarcomere size L and myofibrillar displacement Δ. Each of the (9 × 6) panels is a schematic diagram of 6 segments of myofibrils that are adjacent and parallel respectively along *z* and *x* directions. For each panel, upper half of myofibrils are displaced from the lower half in *x* direction by Δ. Each myofibril is shown with a series of 4 sarcomeres consisting of A-bands (*red* and *blue* color accounting for polarity inversion) alternating with I-bands (*dark* color). Thin band with *grey* color at the center of each A-band corresponds to the M-band region of size m = 150 nm with antiparallel overlapping of myosin thick filaments where no SHG signal is produced. A schematic view of the sarcomere is shown in inset (upper left corner). Theoretical SHG-IP, obtained for a laser beam focalized along the horizontal line at the middle of each panel, is plotted (full lines) with arbitrary units. Note also the scale in μm at the bottom of each column.

#186253 - $15.00 USD Received 5 Mar 2013; revised 19 Apr 2013; accepted 20 Apr 2013; published 2 May 2013
(C) 2013 OSA

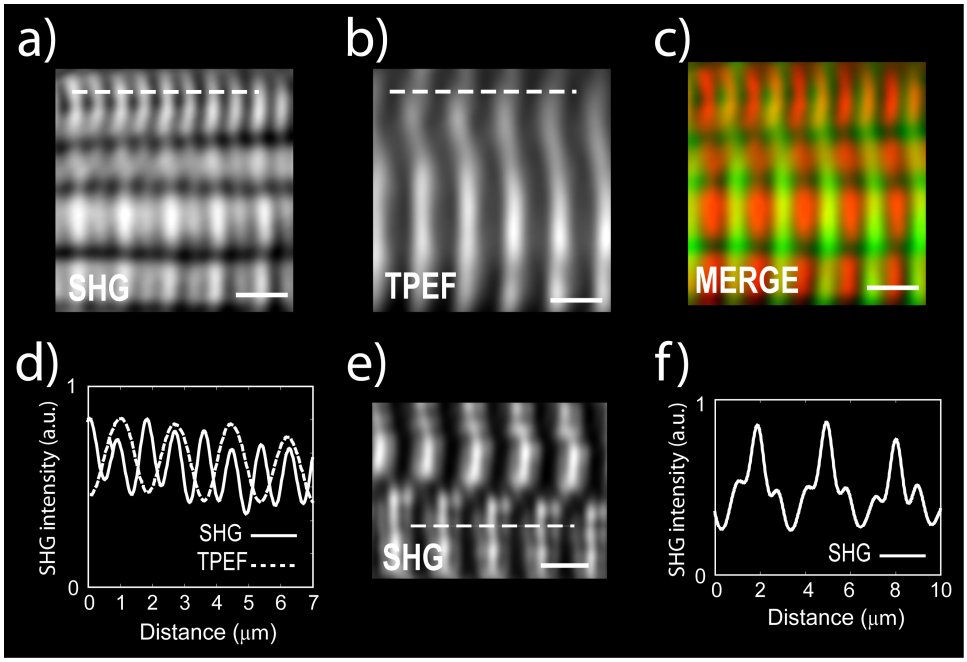


Fig. 4. Experimental SHG, TPEF α-actinin images and SHG-IPs from post-mortem proteolysed muscle. (a) SHG. (b) TPEF. (c) Merge of (a) and (b). Note that the images are from 24 hours post-mortem proteolysed and contracted muscle (L = 1.8 μm). Note also that *red* and *green* colors in (c) are respectively SHG and TPEF images. (d) SHG-IPs along indicated dotted lines of (a) and (b). (e) SHG image from 30% elongated 3 hours mild proteolysed muscle (L = 3.1 μm). (f) SHG-IP along indicated dotted line of (e). Scale bars are 2 μm.

For well-aligned myofibrils ($\Delta = 0$), SHG-IP is 1P for sarcomere size $L \geq 2\mu m$. The over intensity at the M-band (see the schematic view of a sarcomere in the inset of Fig. 3) corresponds to constructive interferences involving intra-thick filaments polarity inversion as previously reported [12].

For hyper contracted sarcomeres ($L = 1.6\mu m$), density of myosin thick filaments is almost constant for any position of the laser beam. In consequence, modulation of the sarcomeric SHG-IP that is observed when Δ varies, is the result of different constructive interference effects involving polarity inversion along x and z directions. For $\Delta = 0$, SHG intensity is lower at the M-band than at the Z-line due to the antiparallel overlapping of myosin tails (*grey* color). For $\Delta \neq 0$, increasing myofibrillar displacement Δ from 0 to L reveals the periodicity of the SHG-IP.

For contracted sarcomeres ($L = 1.8\mu m$), SHG-IP is almost always 2P for any value of Δ. For $\Delta \leq 0.4\mu m$, maximum SHG intensity appears at the M-band and surprisingly at the Z-line which is usually a region with no emitters. That is confirmed experimentally using immuno fluorescence labeling of the Z-line as illustrated in Figs. 4(a)-4(d).

For usual resting sarcomere length ($2\mu m \leq L \leq 2.4\mu m$), increasing myofibrillar displacement Δ from 0 to $L/2$ results in a conversion of the sarcomeric SHG-IP from 1P to 2P.

For elongated sarcomere ($L = 3\mu m$), increasing myofibrillar displacement also results in a conversion of the sarcomeric SHG-IP from 1P to 2P at $\Delta = L/2$. Moreover, additional sarcomeric SHG-IP with three peaks (3P) can be observed for L values ranging from 0.8 to 1.2 μm due to A-band to I-band, A-band to A-band, and I-band to A-band transitions along z

#186253 - $15.00 USD Received 5 Mar 2013; revised 19 Apr 2013; accepted 20 Apr 2013; published 2 May 2013
(C) 2013 OSA

direction. Presence of 3P sarcomeric SHG-IP is also confirmed experimentally as illustrated in Fig. 4(e) and 4(f).

A major conclusion of this theoretical simulation is that sarcomeric SHG-IP can be 1P, 2P or 3P. Number and position of these maxima are driven by both sarcomere size and amount of myofibrillar displacement. Surprisingly, these maxima could occur at position with low density of myosin emitters.

5. Discussion

Theoretical simulation put forward that, depending of the sarcomere size and of the amplitude of myofibrillar displacement, SHG-IP is 1P, 2P or 3P. We have recently shown that direction of emission of SHG light is directly impacted by the spatial modulation of the second-order nonlinear optical susceptibility according to the following condition $\boldsymbol{k}^{2\omega} = 2\xi\boldsymbol{k}^{\omega} + \boldsymbol{G}$ [13]. Indeed, in case of a dominant wave vector $\boldsymbol{G}$ associated to the spatial modulation of the second-order nonlinear optical susceptibility then $g^{f}(\theta,\varphi)$is maximum when this condition is satisfied (see Eq. (3)). Above condition is an extension of the one given by Freund for plane waves $(\xi = 1)$ to describe second-harmonic scattering in collagen tissue [24, 25].

For healthy sarcomeres with well-aligned adjacent myofibrils as shown in Fig. 3 ($\Delta = 0$), sarcomeric SHG intensity peaks are obtained when polarity transition occurs either at the M-band for resting sarcomeres $(L = 2 - 2.4\mu m)$ and both at the M-band and Z-line for hyper contracted sarcomeres $(L = 1.6\mu m)$. This result reveals constructive interferences between harmonic waves originating from hemi A-bands of inverse polarity as previously reported [12, 13]. Indeed, as SHG signal originates only from a small focusing region in *x* direction $1.81 \times w_{xy} \sim 0.8\mu m$ [13] driven by the transversal size of the PSF, polarity inversion occurring over such distance leads to a dominant modulation wave vector component $G_x = 2\pi / (1.81 \times w_{xy}) = 7.2\mu m^{-1}$ that is close to $\sqrt{(k^{2\omega})^2 - 4\xi^2 (k^{\omega})^2} \sim 8\mu m^{-1}$ ($\xi \sim 0.9$ in our experimental conditions), the necessary modulation wave vector achieving above condition as shown in Fig. 5(a). SHG signal is emitted off axis with an angle given by $\theta = \tan^{-1}(G_x / 2\xi k^{\omega}) \sim 24°$. Constructive interferences between harmonic waves emitted from opposite charges within the PSF occur because their optical path difference δ is close to $\lambda_{2\omega} / 2$ which compensates phase mismatch due to polarity inversion [12].

For mild proteolysed muscle tissue characterized by myofibrillar displacement as shown in Fig. 3 ($\Delta \neq 0$), sarcomeric SHG intensity peaks are often localized at positions where hemi A-bands with inverse polarity are aligned along *z* direction. Once again, as SHG signal originates from a small focusing region $1.81 \times w_z \sim 4\mu m$ in *z* direction driven by the axial size of the PSF [12, 13], polarity inversion occurring over such distance leads to a dominant modulation wave vector component $G_z = 2\pi / (1.81 \times w_z) = 1.4\mu m^{-1}$ that is close to $\left| k^{2\omega} - 2\xi k^{\omega} \right| = 1.8\mu m^{-1}$, the necessary modulation wave vector achieving above condition as shown in Fig. 5(b). As fundamental and harmonic waves propagate in the same *z* direction, constructive interferences between harmonic waves radiated by opposite charges within the PSF occur because mean distance $d = \frac{1}{2}(1.81 \times w_z) \sim 2\,\mu m$ between these dipoles is close to the coherence length $L_c = \pi / \Delta k \sim 1.7\mu m$ with $\Delta k = k^{2\omega} - 2\xi k^{2\omega} \sim 1.8\,\mu m$ [26]. Such constructive interferences obtained along the main direction of propagation of the incident IR beam for mild proteolysed muscle tissue, is reminiscent of polarity inversion occurring every coherence length that has been used to enable quasi-phase-matching between fundamental and harmonic waves in periodically poled ferroelectric materials [27].

#186253 - $15.00 USD Received 5 Mar 2013; revised 19 Apr 2013; accepted 20 Apr 2013; published 2 May 2013
(C) 2013 OSA

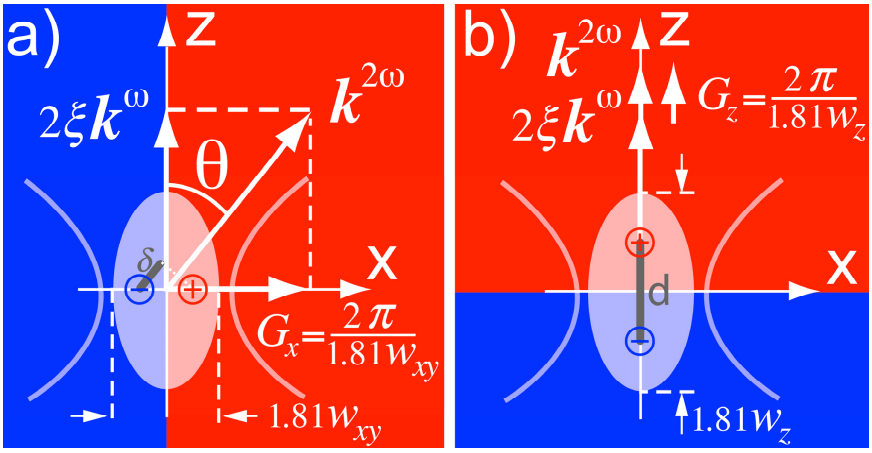


Fig. 5. Wave vector diagrams representing well aligned (a) and misaligned (b) sarcomeres. Laser beam is focused (PSF in *white* color) at the transition between two regions of inverse polarity as shown by the *red* and *blue* color transition. (a) Polarity inversion is along *x* direction. Mean distance between charges of opposite polarity within the PSF is $\frac{1}{2}\times 1.81 w_{xy}$. Optical path difference between harmonic waves emitted at θ angle is $\delta = \frac{1}{2}\times 1.81 w_{xy} \times \sin(\theta)$. (b) Polarity inversion is along *z* direction. Mean distance d between charges of opposite polarity within the PSF is $d = \frac{1}{2}\times 1.81 w_z$.

This study shows that SHG-IP enables the mapping of myofibrillar displacement without any labeling. This technique could be used to image and quantify disruption of the excitation contraction coupling [14, 15] due to structural myofibrillar disorganization as observed in several animal and human skeletal muscle gene diseases [16–18].

6. Conclusion

This report shows that myofibrillar displacement results in the conversion from 1P to 2P or 3P sarcomeric SHG intensity pattern (SHG-IP) due to interference effects in the focusing volume involving polarity inversion between emitters. We anticipate that sarcomeric SHG-IP tool, which enables the mapping of myofibrillar displacement without any labeling, will be of paramount to study the spatial correlation between myofibrillar disorganization and excitation-contraction disruption occurring in physiological adaptation and muscle disease.

Acknowledgment

This work was supported by Région Bretagne, Rennes Métropole, Conseil Général d'Ille-et-Villaine, CRITT Santé Bretagne and Ministère de l'Enseignement Supérieur et de la Recherche. We also thank Régis Morel for its technical assistance.

#186253 - $15.00 USD Received 5 Mar 2013; revised 19 Apr 2013; accepted 20 Apr 2013; published 2 May 2013

(C) 2013 OSA